Thermochimica Acta, 61 (1983) 341–356
Elsevier Scientific Publishing Company, Amsterdam – Printed in The Netherlands

DECOMPOSITION OF LEAD(II) 2,4-DINITRORESORCINATE. THERMOGRAVIMETRY, CALORIMETRY, MICROSCOPY AND TIME-RESOLVED MASS SPECTROSCOPY

TONG B. TANG

Physics and Chemistry of Solids Group, Cavendish Laboratory, Cambridge (Gt. Britain)

(Received 17 August 1982)

ABSTRACT

An experimental study has been made on the solid-state decomposition of lead dinitroresorcinate under the action of heat. This material is an ionic compound which finds practical use as an explosive. The stoichiometry of its pyrolysis was investigated with mass spectrometry and IR spectroscopy. Isothermal thermogravimetric experiments were carried out at various temperatures between 220 and 250°C to determine the kinetics. The principal activation energy was found to be 1.8 eV. The enthalpy change was measured as 380 kJ $mole^{-1}$ by means of differential scanning calorimetry and the developmental morphology observed with a scanning electron microscope. Suggestions concerning reaction schemes were based on the identification of transient species from mass spectra obtained continuously at a high scanning speed and recorded on video tapes. It appears to be the first time that this method has been applied for such a purpose.

INTRODUCTION

A primary explosive discovered in the last century [1], lead(II) 2,4-dinitroresorcinate (hereafter denoted by PbDNR), has been employed since 1940 as an ingredient of cap and delay compositions in electric detonators and certain special designs of ammunition. Nevertheless, so far no basic study on its pyrolysis has been reported. An additional motivation for the present work arose from the observation that, like silver, thallous and lead azides and lead styphnate [2], it explodes when subjected to a strong electric field: a behaviour which may perhaps be explained by the occurrence of slow decomposition under the action of the field. This paper describes experimental results on the thermochemistry, stoichiometry, kinetics and morphology of its slow thermal decomposition.

Some clarification has also been sought on the nature of elementary steps in the reaction. Time-resolved mass spectrometry has proved valuable for this purpose. The technique has been applied to flash and laser photolyses as pioneered by Norrish and Porter (e.g., ref. 3) and, once, to fracture-induced

0040-6031/83/0000–0000/$03.00

decomposition [4]. Of course, in the present case the pyrolysis takes place in the solid state. Still, the possibility exists that helpful information can be gained, if in the process under study there are intermediate chemical species, of sufficiently long lifetimes in the solid, which may occasionally be ejected due to reaction exothermicity. The mass spectrometer needs to operate at high resolution in time to detect these transient species: because their evolution is intermittent, their partial pressures will be reduced by a large factor when averaged over a long time interval. Since synchronization between decomposition events and mass scans cannot be arranged, the latter are made continuously and repeatedly at a high speed. A novel feature of experimental implementation is perhaps in data storage by a video camera-recorder system. The dynamic spectrometer employed is a quadrupole. Time-of-flight instruments can be even faster but are more expensive and ultrahigh speeds will also prevent the use of an ordinary video recorder.

PbDNR is an essentially ionic compound and has the structural formula

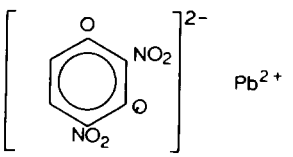

The 4,6-isomer is of less interest due to the difficulty in its synthesis, although its basic and acid salts do exist and are used. The closely related trinitroresorcinate, $Pb[O_2C_6(NO_2)_3H]$, is what has been referred to by the common name of (α-) lead styphnate. Containing one more nitro group, the styphnate is more brisant than PbDNR but at the same time more sensitive to impact. KDNR and NaDNR, on the other hand, are less sensitive, like most Group IA metal-substituted compounds in general. Recently they have received attention as promising safer explosives, and the present work may be relevant as part of a systematic study of DNR salts.

EXPERIMENTAL

Material

PbDNR was obtained as a brownish red powder of rounded granules from Propellants, Explosives and Rocket Motor Establishment at Waltham Abbey, England. Prior to utilization the powder had been stored in the dark for about 3 years. According to the specifications provided, the major impurities were acetate ($\leqslant 0.7\%$) and metals ($\leqslant 0.3\%$) which, from energy dispersive X-ray analysis, were found by this author to be mainly Na, Ca and Fe. The particle size distribution was determined by means of optical microscopy as $100(+200-50)\ \mu m$.

Differential scanning calorimetry

Three experimental runs were made on a Dupont 910 differential scanning calorimeter, all at heating rates of 5 K min^{-1} from 50 to 200°C and then 2 K min^{-1} at 200–300°C. Sample pans were made of aluminium and an empty pan served as the reference; the ambient was dried argon flowing at 70 ml min^{-1}. The calibration of the calorimeter and chart recorder assembly was verified against the fusion of indium standard supplied by Perkin-Elmer. PbDNR and indium samples all had masses within 1–2 mg, obtained on the same balance (the TG-750 mentioned below).

The specific heat and the enthalpy of decomposition, at constant pressure, were calculated from the thermograms. No kinetic analysis was attempted as isothermal experiments had not been performed.

Product characterization

The gases produced when PbDNR decomposed were monitored in an ultrahigh vacuum system to which an ion pump and a quadrupole spectrometer (Vg Micromass QX-200) were attached. The powder was held between the coils of a tantalum foil that was wrapped around the end of an alumina tube. The tube was screwed to a linear motion drive so that, when so desired, the sample could be put through a hole of a furnace to rest at the centre where a Pt–Pt 13% Rh thermocouple was placed. The spectrometer's ionizer sat opposite another hole of the furnace, at a distance of 45 mm to the centre. Ionizing potential and emission current were 70 V and 0.5 mA, respectively.

Two alternative procedures were followed in recording mass spectra. In the first, at the start of the pyrolysis the vacuum system was isolated from the pump by the closing of a valve. The spectrometer was operated with a Faraday bucket as its collector, the output of which was fed via a Keithley 610B electrometer to a chart recorder. In the second procedure, fast-scanned spectra were observed with the isolation valve left open. The spectrometer worked in electron-multiplier mode and its output was displayed directly on a Tektronix 7704A oscilloscope (with short-persistence P11 phosphor) incorporating a 7A22 plug-in amplifier (optimum bandwidth setting at DC to 10 kHz). Data storage at the normal rate of 50 spectral frames per second was achieved with a Shibaden HV-40SK camera and a Sony CV-2100ACE video recorder. Individual frames were retrieved consecutively by advancing the video tape manually.

Both the fresh material and the solid product remaining after complete decomposition were examined by IR spectroscopy and X-ray diffraction. Spectra were taken in nujol mulls. X-ray patterns in the NiK_α line were taken with a powder camera.

Thermogravimetry

A Stanton-Redcroft TG-750 thermobalance was employed to investigate the kinetics. Eight isothermal runs were carried out at temperatures in the range 220–250°C. A data logging system stored weight readings on tape regularly at a selected frequency; the resolution in the recording reached 1 in 1999 but the signal-to-noise ratio remained the limiting factor. In each run an empty pan was first lowered into the pre-heated furnace, and the transient so obtained subsequently subtracted from the initial part of the weight loss curve recorded when the pan was again lowered with the sample in it.

Scanning electron microscopy

The morphology of the decomposition process was studied in a Cambridge Stereoscan S4-10 operated at 30 kV. Secondary electron micrographs were taken of PbDNR particles transferred from the thermobalance after reaching various degrees of conversion. The final residue, after being treated in dilute hydrochloric acid or after being heated to 980°C, the maximum temperature attainable in the thermobalance, was also examined.

RESULTS

Thermal and thermochemical properties

TABLE 1

Specific heat capacity, C_p (estimated standard error, $\pm 3\%$) and enthalpy change of decomposition, $\Delta H(\pm 5\%)$

T(°C)	C_p(kJ K^{-1} $mole^{-1}$)
60	0.36
80	0.39
100	0.41
120	0.42
140	0.43

$\Delta H(495-550\ K) = -380$ kJ $mole^{-1}$.

Stoichiometry

The first sample which was heated in the mass spectrometric system to 220°C exploded after 10 s. The second sample was heated at 186°C. The relative abundance of evolved species was measured successively five times

TABLE 2

Permanent gaseous species evolved from PbDNR decomposing at 186°C

Mass-to-charge ratio	18	28	44	2	12	14	16	17	30	32
Relative intensity of ion current	1	1.0	1.2	0.1	0.1	0.05	0.1	0.2	0.1	0.05
(±0.02)	±0.5							±0.2		

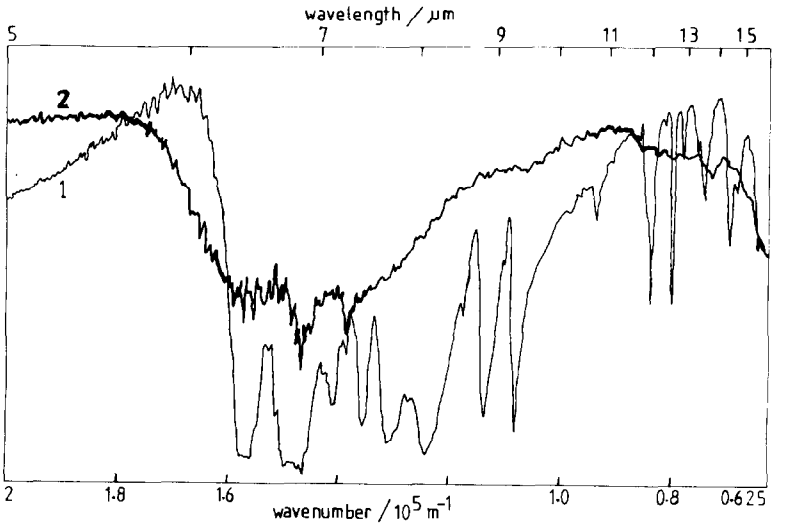

Fig. 1. Infrared spectra of (1) fresh, and (2) decomposed PbDNR.

with the 'steady state' procedure and found to be quite constant: the mean distribution is given in Table 2.

The peak at m/e equals 44 should correspond mainly (though probably not exclusively) to CO_2^+; the cracking pattern of N_2O includes a 31% subsidiary peak at 30, which in the present case is tiny. After being corrected for instrumental sensitivity factors ($CO_2^+ = 1$, $N_2^+ \equiv 1$, $H_2O^+ = 1.2$) and the 11% contribution by CO_2 to the peak at 28, the relative partial pressures of principal gaseous products are consistent with the reaction scheme

$$Pb(O_2C_6(NO_2)_2H_2) \rightarrow PbO_2 + \tfrac{9}{2}\,C + \tfrac{3}{2}\,CO_2\uparrow + H_2O\uparrow + N_2\uparrow$$

TABLE 3

Strong absorption peaks in IR spectrum of PbDNR

Wave number (cm^{-1})	Probable assignment
695	$-NO_2$ in-plane bending
740	$-NO_2$ out-of-plane bending
835	⎓C–N vibration
880	⎓C–H out-of-plane bending
1085	⎓C–H in-plane bending
1240, 1310	⎓C–O stretching
1350	$-NO_2$ symmetrical stretching
1500	C⎓C stretching
1460, 1560–80	C⎓C in-plane bending

This scheme predicts a mass loss of 27%, in reasonable agreement with the empirical figure of $24 \pm 1\%$ from thermogravimetric experiments. The discrepancy may be due to additional retention of some products, nitrogen for example, in certain forms at advanced stages of decomposition. The constancy of the ratio between 44 and 28 peak heights implies the same of reaction stoichiometry, at least during the early stages. The relatively large variation at 18 is probably caused by water desorption from the sample holder.

The solid residue was found to be a black powder; the usual colours of both PbO_2 and C are indeed black. Its IR spectrum, given in Fig. 1 (trace 2), confirms complete decomposition since all the absorption bands given by the fresh material [Fig. 1 (trace 1), and Table 3] have disappeared entirely. At the same time, this spectrum reveals the remainder of certain C–C bonds, as shown by the broad absorption band of 6.3–7.3 μm, and is thus indicative of residual aromaticity. Moreover, its X-ray diffraction pattern was seen to consist solely of a diffuse ring corresponding to $d \approx 3.5$–4.8 Å. The conclusion may be drawn that its structure is complicated and on the whole amorphous.

Intermittent pathways

The presence of additional gases, namely H_2, NO, O_2 and N_2O, in trace quantities as seen from Table 2 suggest that decomposition infrequently

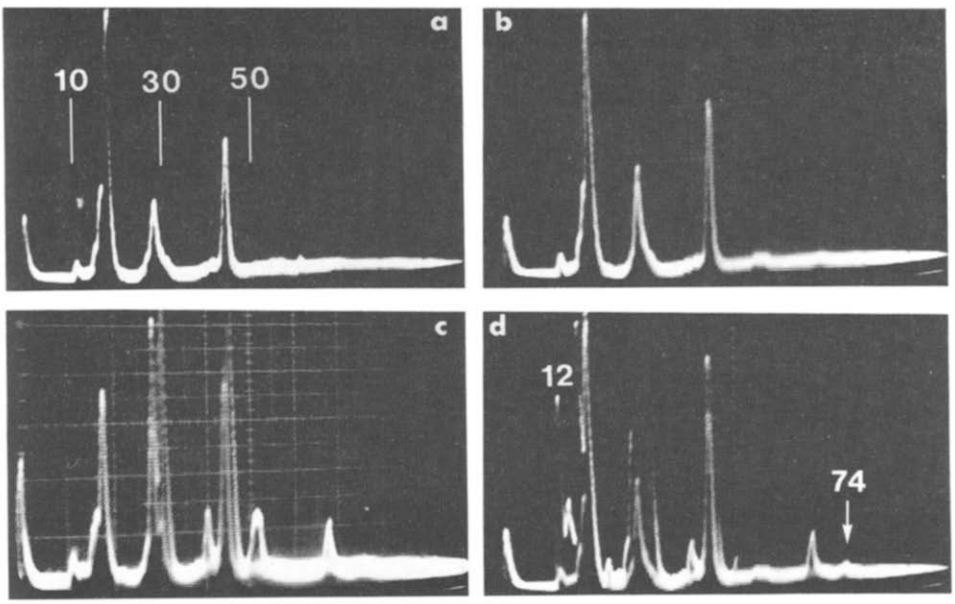

Fig. 2. Mass spectra relating to (a) background of vacuum system, and (b, c, d) PbDNR decomposing at 177°C. Scan speed at 1 amu per 0.3 ms. Note that (d) is a double exposure of two consecutive spectra, possible because, on the TV screen, two fields, comprising the odd and even lines, respectively, are scanned alternately.

occurs along other chemical pathways ending in different products. Mass spectrometry undertaken at a high scanning speed and with the system continuously evacuated has made it possible to speculate on intermittent reaction schemes. Individual bursts of gaseous evolution were registered when a third sample was heated at 177°C. The majority gave spectra consistent with the main scheme already described, an example being Fig. 2(b). Very occasionally, however, more complex patterns appeared.

The spectrum of Fig. 2c has been selected for illustration here as it demonstrates the complexity in a pure form. Compared with the preceding spectrum taken nominally 20 ms earlier, it shows no significant increases at 44 and 18; most of the other complex patterns recorded include rises indicative of decomposition according to the main scheme running concurrently, as in Fig. 2d. On the other hand, increases in intensity are discernable at 68, 52, 46, 40, 30, 28, 16, 14 and 2.

Those at 46, 30, 16 and 14 are in the ratio, measured more accurately on other spectra, of 10 : 20 : 2 : 1 which fits the cracking pattern of NO_2. In one case these increases could be made out before change occurred at any other peak. Since in a mass scan 30 and 46 are reached before 52 and 68, the absence of peaks at the latter positions cannot be explained away as due to the finite speed of scanning. There is therefore some tentative evidence for the proposal that the reaction follows intermittent pathways when NO_2^- ($-NO_2$ having strong electron-withdrawing power) on breaking lose manages to lose its electron. It then leaves the surface and can be picked up by the spectrometer but, on longer time-scales, becomes NO, O_2 and N_2O. Left behind in the solid is $[O_2C_6H_2]$.

The rise at $m/e = 2$ can be unambiguously ascribed to H_2^+. The remaining four peaks at 68, 52, 40 and 28 might be associated with $[C_2N_2O]$, cyanogen, $[CN_2]$, and nitrogen, but their formation is most unlikely. Instead, we may envisage that $[O_2C_6H_2]$ is indeed formed and divides into $[C_3O_2] + 3\,C + H_2\uparrow$. Supposedly a few ring fractions are occasionally thrown out because of reaction exothermicity and, together with their fragments in the electron beam namely C_3O^+, C_2O^+ and CO^+, are responsible for the four peaks.

Metastable species

The spectrum in Fig. 2(d) is a superposition of those in Fig. 2b and c: in this respect it is typical of the complex patterns. But it includes, as a minority of other spectra do, a tiny peak at 74 and a strong one at 12. The most natural explanation is in terms of $[C_6H_2]$, and C which comes from the disintegration of the former in the electron beam of the spectrometer.

No peaks have ever been detected in the m/e range 75–210. The absence of Pb^+ or Pb^{2+} is a proof that the thermal decomposition takes place in the solid state and that the large fragments deduced from the complex spectra do not arise from vaporization followed by electron-beam decomposition.

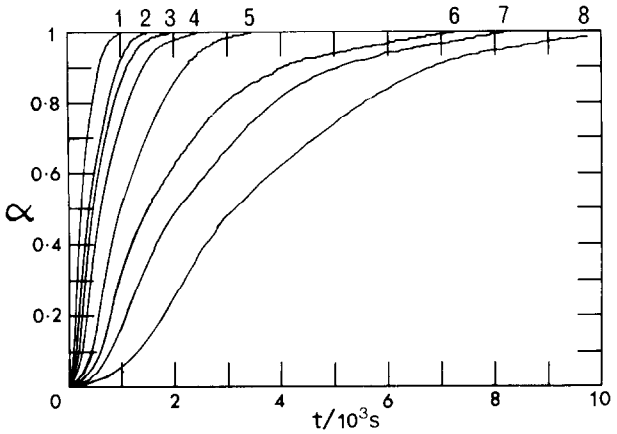

Fig. 3. Fractional decomposition as isothermal functions of time. Tracing of computer generated curves. The temperatures were 250, 244.5, 242, 239, 233, 228.5, 224 and 220°C for curves 1–8, respectively.

Kinetics

Weight loss traces obtained with dried argon flowing at 20 or 50 ml min^{-1} as the dynamic atmosphere in the thermobalance were found to lack sufficient reproducibility and to give final loss varying from 23 to 29%. They resemble the curves in Fig. 3 except that, corresponding to a given temperature, the trace shows a much steeper rise until 'α' reaches just above 0.8 and thereafter flattens more or less abruptly. The solid residue was dull red in

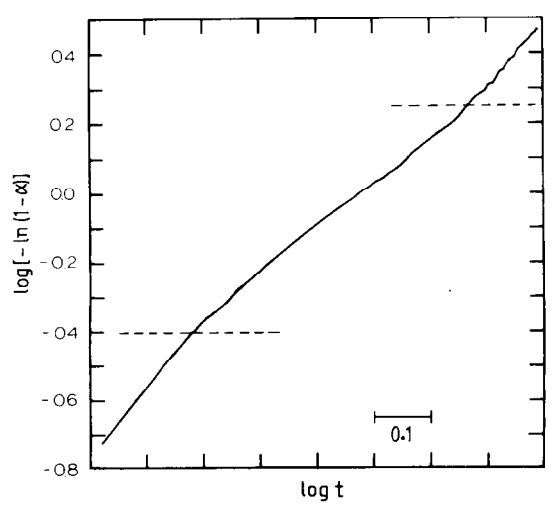

Fig. 4. Log–ln plot of data obtained at 242°C.

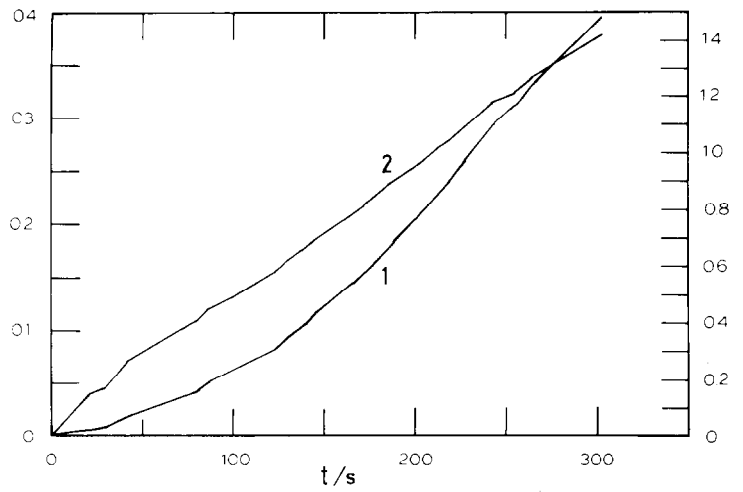

Fig. 5. Graphs of (1) α, and (2) $2[-\ln(1-\alpha)]^{1/2}$, vs. time, with scales (1) on the left and (2) on the right, respectively.

colour, and the use of a nitrogen atmosphere at the same flow rates led to similar results. Data discussed below were obtained with argon flowing at 70 ml min^{-1}.

Final weight loss was measured as $24 \pm 1\%$. The data were analyzed by a computer programme that implemented a method proposed previously [5]. The digital gravimetric readings were converted into α–t curves (Fig. 3) where $\alpha \equiv$molar fraction of decomposition at time t. Partial noise reduction was achieved by truncation of any negative going transients. Next, plots of

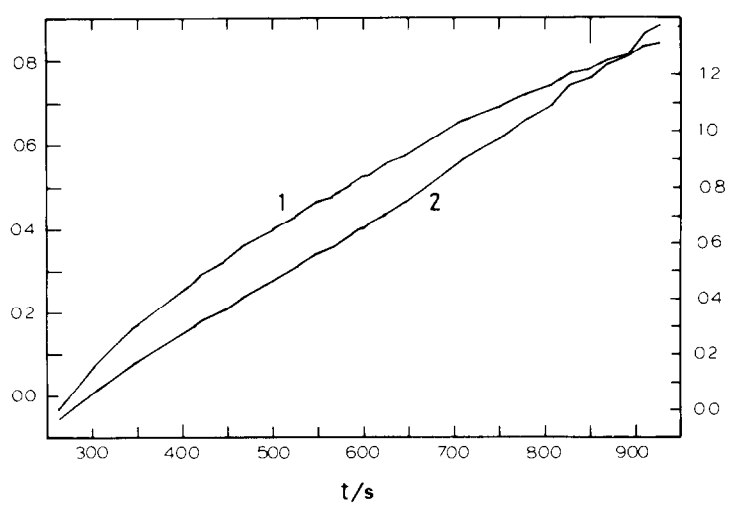

Fig. 6. Graphs of (1) α', and (2) $3[1-(1-\alpha')^{1/3}]$, where α' is adjusted fractional decomposition as explained in the text, with scales for (1) and (2) on the left and the right, respectively.

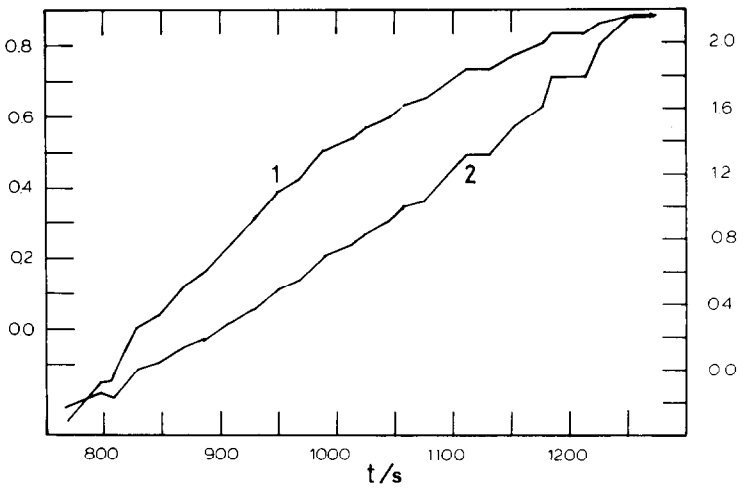

Fig. 7. Graphs of (1) α'', and (2) $-\ln(1-\alpha'')$.

$\log[-\ln(1-\alpha)]$ vs. $\log t$ were generated, a typical example being shown in Fig. 4. In the beginning all were virtually straight lines with the same slope of 2.0, implying that the α–t curves could be fitted by the Avrami–Erofeev expression of exponent two. The implication was confirmed by the linearity of $2[-\ln(1-\alpha)]^{1/2}$ vs. t graphs until α reached about 0.35, as in Fig. 5.

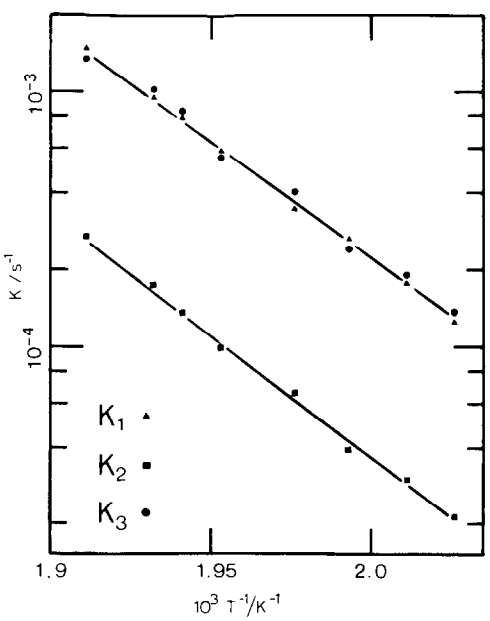

Fig. 8. Arrhenius plot of rate constants for the three successive stages of PbDNR decomposition.

Maximum $d\alpha/dt$ was found at $\alpha = 0.30 \pm 0.03$ in general.

Subsequent parts of the TG curves where α exceeded 0.35 were analyzed again, after the adjustment of α to $(\alpha - 0.35)/(1 - 0.35)$, t to $t - t$(when $\alpha = 0.35$) was done to correct for the fraction already decomposed in the preceding stage [6]. The beginning sections of $\log[-\ln(1-\alpha')]$ vs. $\log t'$ plots were all found to have a slope of approximately 1. This condition suggested the Avrami–Erofeev function of index one, or one of the contracting envelope types, as $1-(1-\alpha')^{1/n} \approx 1 - 1 + \alpha'/n \propto \alpha' \approx -\ln(1-\alpha')$, for small α'. After the data had been analyzed according to each in turn, it was determined that for α up to about 0.85 the curves were best described by the

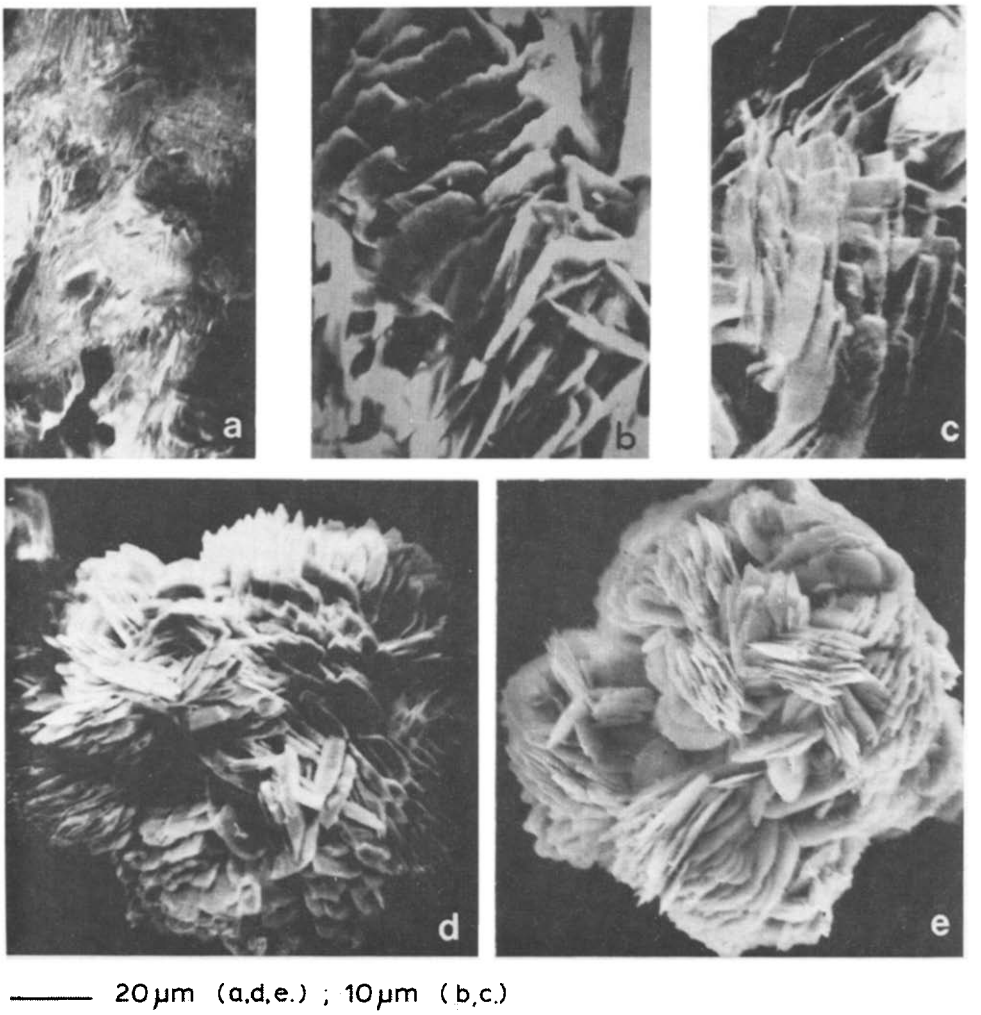

Fig. 9. PbDNR particles of fractional decomposition (a) about 0.005, (b), 0.03, (c) 0.05, (d) 0.25, and (e) 1.0.

contracting volume equation. The analysis of α''–t'' curves, where $\alpha'' = (\alpha - 0.85)/(1 - 0.85)$ and $t'' = t - t$(when $\alpha = 0.85$), in turn led to the (apparent) first-order law as the best fit. Figures 6 and 7 illustrate the two cases respectively. In summary, the following kinetic laws have been identified

$0 < \alpha < 0.35$	Stage I	$2[-\ln(1-\alpha)]^{1/2} = K_1 t$
$0.35 < \alpha < 0.85$	Stage II	$3[1-(1-\alpha')^{1/3}] = K_2 t$
$0.85 < \alpha < 0.95$	Stage III	$-\ln(1-\alpha'') = K_3 t$

Above $\alpha \approx 0.95$ the quality of the data was inadequate for any reliable interpretation to be asserted.

The logarithms of rate constants, K, are plotted against reciprocal absolute temperatures in Fig. 8. The derived activation energies and pre-exponential factors are, successively:

K_1: 1.8 eV($\pm$8%), 3×10^{14} s ($\pm$30%)

K_2: 1.9 eV($\pm$8%), 5×10^{14} s ($\pm$30%)

K_3: 1.8 eV($\pm$15%), 3×10^{14} s ($\pm$60%)

Morphology

PbDNR particles of low fractional decomposition showed charge accumulation effects when examined in high magnification under the microscope. The instrument model used did not allow operation at a low voltage, which would have reduced the effects; nor was deposition of metallic film to

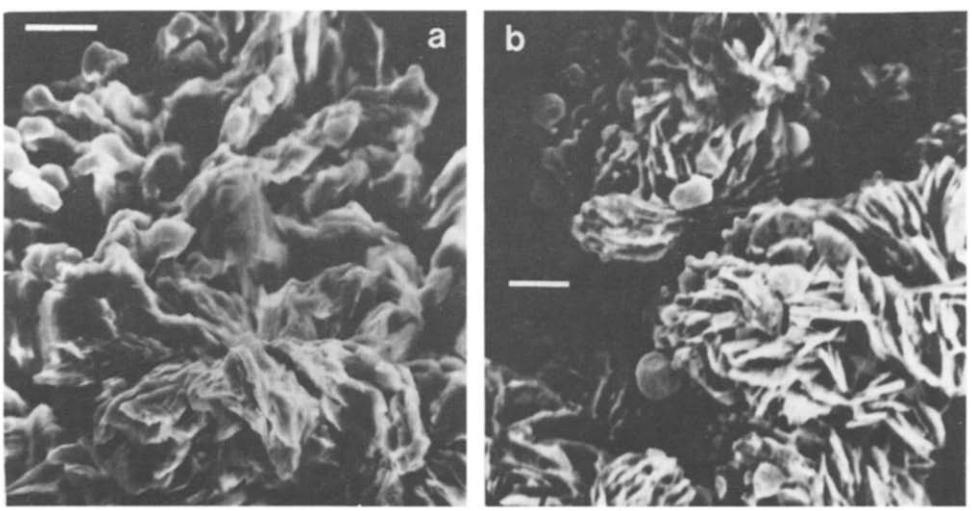

Fig. 10. Solid residue after (a) treatment in dilute hydrochloric, or (b) heating at 980°C for 5 min. Scale bars represent 10 μm.

eliminate the effects desirable as it would have caused appreciable surface decomposition. Fortunately, sudden movements of the particle under the beam were prevented when a layer of carbon-dag was thinly spread on the specimen stud and allowed to dry almost completely before the particles were sprinkled on top. Also, images recorded at fast scan times (4 s at $\times 1000$ or $\times 2000$) were often free from fictitious contrast. A completely decomposed sample conducted quite well, as very little charge accumulation was measured when the specimen stud was earthed through a nanoammeter. The presence of free carbon is a good explanation for the high conductivity.

Figure 9 shows a sequence of micrographs of particles decomposed to various extents. The decomposing surfaces are inferred from their plate-like appearance. They exist first at isolated locations on the surface (micrograph a), then they grow in length and depth (b) so that the entire surface becomes decomposed (c and d). The reaction thus proceeds radially only. They are oriented in the same crystallographic direction within what presumably are individual grains of the original particle.

The residue from a sample decomposed at 220°C was treated in dilute HCl. Evolution of gases was apparent but stopped after a few seconds. From Fig. 10a one notes that the acid has dissolved only the sharp edges of the residue particles, an observation consistent with the assumption that PbO_2 (soluble) and C (insoluble) in an intimate (disorganized) form comprise the residue. Another sample which had been decomposed at 233°C was further heated to 650°C at 5 K min^{-1} in a flowing argon atmosphere. Its weight dropped continuously and stayed quite steady only after it had been at 650°C for some 3 h, when the total weight reduction was about 25%. The reason may be the conversion of PbO_2 into Pb_3O_4 and then β-PbO, accompanied by the oxidation and subsequent loss of some carbon. It became a yellow powder mixed with a tiny amount of black particles; massicot does look yellow in colour and carbon should of course be black. Figure 10b shows the formation of lead particles (as inferred from the intensity distribution of the lead L_α line in EDXA) after it was kept at 980°C for 5 min.

DISCUSSION

The observations just described, together with the IR and X-ray results, tend to support the view that the (amorphous) residue consists of lead dioxide and (in part polycyclic) carbon phases. The production of the dioxide in the presence of a reducing agent would have seemed surprising but for the fact that the two are in a complicated form. On heating, lead styphnate is known to yield similarly a black amorphous solid, the chemical composition of which is undetermined, however [7].

The micrograph sequence points to an initiation of decomposition from a fixed number of sites on the surface. A constant number of nucleation sites is indeed expected as the material is well aged. The reaction then proceeds

anisotropically across and inwards along certain crystallographic planes. This agrees with the fact that the Avrami–Erofeev expression of exponent two fits the kinetic data during the first stage. The decrease of the reaction velocity, $d\alpha/dt$, after $\alpha = 0.30 \pm 0.03$ may be attributed to interference in growth of nuclei. At $\alpha \approx 0.35$ the kinetic law changes into the contracting sphere type. The transition may be interpreted as the onset of complete coverage of the undecomposed part, by the solid product that has penetrated to $(1 - 0.35)^{1/3}$ or 0.87 radius. Further consumption of the reactant then advances in a shell by shell manner. By $\alpha \approx 0.85$, corresponding to about 0.53 radius, the probability of reaction becomes apparently independent of location, probably because by then the reactant is extensively fractured.

The slopes of the log–ln plots, or 'apparent Avrami indices' m, in the three stages discussed above are 2.0, 1 and 1.0, respectively. This conforms with the general rule that m must decrease or at most remain constant when one stage succeeds the other, otherwise compatible physical interpretations [6] cannot be made. The plate-like appearance of the solid product means that decomposition is very slow in the perpendicular direction. Of the other two crystallographic orientations, the inward direction is that along which decomposition is less fast, as suggested by the slightly higher activation energy during the second stage.

Time-resolved mass spectrometry has identified the gaseous products and some long-lived transient species. They may be accounted for by the following two reaction schemes. However, much more work involving, for example, isotope labelling and metastable or desorption ionisation spectrometry is needed to establish the validity of these schemes. The spectrometry technique may itself also be further refined, with the use of more expensive instrumentation, enabling higher time resolutions to be attained. Recording may be done with the help of 2000 frames s^{-1} video recorders and nanosecond decay time phosphor (such as the 102A from Nuclear Enterprises Ltd.) that are commercially available.

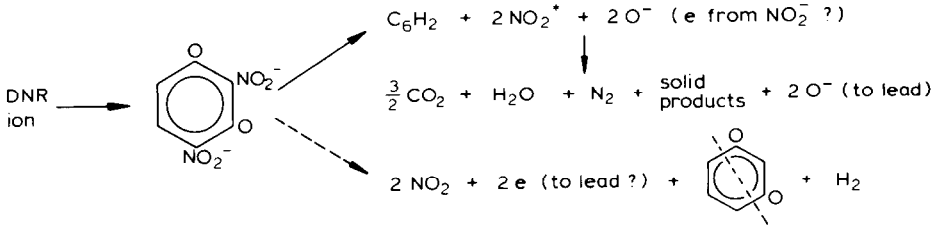

For a PbDNR charge of the single crystal density of 3.2 g cc^{-1}, it follows from the results reported here that 3 kJ of heat and, according to the main reaction scheme, 1.7×10^{22} gas molecules are produced per cc. This strength of slow deflagration is about two-thirds of that of lead styphnate. It is plausible that PbDNR slowly decomposes under a strong electric field, in common with silver azide [2]. As the solid product, unlike the parent

material, has high electrical conductivity, joule heating can eventually become significant, resulting in fast thermal decomposition. This may be the cause of field-induced explosion.

ACKNOWLEDGEMENTS

I am indebted to Drs. M.M. Chaudhri for encouraging me to try the time-resolved mass spectrometric experiments, J.E. Field for his interest in the work, V. Krishna Mohan for comments on the manuscript and G.M. Swallowe for taking the X-ray diffraction picture. The work was supported by the Procurement Executive, Ministry of Defence, the award of Charles and Katherine Darwin Research Fellowship from Darwin College, Cambridge and the subsequent grant of Senior Membership from Wolfson College, Cambridge.

REFERENCES

1 F.K. Beilstein, Handbuch der Organischen Chemie, Springer, Berlin, 1st edn., 1881, p. 885.
2 T.B. Tang, Ph. D. thesis, Cambridge University, 1979.
3 S.E. Appleby, S.B. Howarth, A.T. Jones, J.H. Lippiatt, W.J. Orville-Thomas, D. Price and (in part) P. Heald, in D. Price and J.E. Williams (Eds.), Dynamic Mass Spectrometry, Vol. 1, Heyden, London, 1970, p. 37.
4 P.G. Fox and J. Soria-Ruiz, Proc. R. Soc. London, Ser. A, 317 (1970) 79.
5 T.B. Tang and M.M. Chaudhri, J. Therm. Anal., 17 (1979) 359.
6 T.B. Tang, Thermochim. Acta, 41 (1980) 133.
7 T.B. Flanagan, Trans. Faraday Soc., 57 (1961) 797.